IN-34-CR
128102
29P.

WASHINGTON UNIVERSITY
DEPARTMENT OF PHYSICS
LABORATORY FOR ULTRASONICS
St. Louis, Missouri 63130

"Quantitative Non-Destructive Evaluation of Porous Composite Materials Based on Ultrasonic Wave Propagation"

Semiannual Progress Report: September 15, 1987 - March 14, 1988

NASA Grant Number: NSG-1601

Principal Investigator:

Dr. James G. Miller
Professor of Physics

The NASA Technical Officer for this grant is:

Dr. Joseph S. Heyman
NASA Langley Research Center
Hampton, Virginia

I. INTRODUCTION

This Progress Report summarizes our continuing research into the quantitative nondestructive evaluation of composite materials. In the September 1987 Progress Report we have described preliminary investigations carried out to characterize porosity in composite media using ultrasonic waves. In this Progress Report we will compare two complementary ultrasonic techniques, transmission mode and polar backscatter, for their potential application to the characterization of porosity in composite laminates. These investigations are described in Section II. Previous reports have also described our investigations of local approximations to the Kramers-Kronig relations. The Kramers-Kronig relations provide a relationship between the frequency dependent attenuation coefficient and phase velocity. In Section III of this Progress Report we present results from the application of this approximation to porous epoxy in order to obtain a prediction of the dispersion from the frequency dependent attenuation coefficient. The estimate of dispersion obtained from the local approximation was found to agree well with the directly measured dispersion. In a more sensitive test of the local approximation in which the excess dispersion of porous epoxy relative to pore-free epoxy was determined from the corresponding excess attenuation coefficient, the predicted and directly measured values of excess dispersion were in good agreement.

II. CHARACTERIZATION OF POROSITY IN GRAPHITE/EPOXY COMPOSITE LAMINATES WITH POLAR BACKSCATTER AND FREQUENCY DEPENDENT ATTENUATION

The goal of this research was to evaluate two complementary ultrasonic techniques for characterizing porosity in fiber-reinforced composite laminates. Five uniaxial graphite-fiber/epoxy-matrix composites having a range of 1% to 8% volume fraction of solid glass inclusions to model porosity were investigated. In one technique, signal loss was measured in transmission mode and the slope of attenuation, obtained from the first order coefficient of a two-parameter polynomial fit about the center frequency of the useful bandwidth, was used as the ultrasonic parameter to characterize the "porosity". The results of these transmission mode measurements displayed a good correlation between the volume fraction of "porosity" and the slope of attenuation. Integrated polar backscatter was used as a second ultrasonic parameter for the characterization of the "porosity" in these samples. A single transducer insonified the samples and measured the resulting backscatter at a polar angle of 30° with respect to the normal of the sample surface with the azimuthal angles centered at 0° with respect to the fiber orientation (i.e., along the fibers). Integrated polar backscatter also displayed a good correlation with the volume fraction of "porosity".

EXPERIMENTAL METHODS

A. SAMPLE PREPARATION

The effects of porosity were simulated by introducing solid glass beads, having a distribution of diameters ranging from 75 to 150 microns, into a 16 ply uniaxial graphite-fiber/epoxy-matrix composite. The composite was fabricated at NASA Langley Research Center using 5208-T300 prepreg tape. Measured amounts of glass beads were introduced between the 12th and 13th layers during the lay-up of a 12 by 16 inch laminate. The beads were dusted onto circular regions 2 inches in diameter at sites on a square grid with centers 4 inches apart. The sample was autoclaved and cured in an oven using a standard cure protocol. The 12 by 16 inch sample was cut into smaller samples (approximately 3.75" by 3.75") so that each contained a single zone of "porosity" with a volume fraction of 1%, 2%, 4%, 6%, or 8%. The bleeder cloth impressions were removed by polishing the top and bottom surfaces of the samples, as suggested by Bar-Cohen.[1]

B. MEASUREMENT METHODS

1. Transmission Mode Measurements

The signal loss was measured in transmission mode with a specimen placed in the overlapping focal zones of a matched pair of 25 MHz center frequency, 0.25 inch diameter, 1 inch focal length transducers. Each sample was scanned on a 21 by 21 grid in 1 mm steps and the acquired frequency spectra were averaged to reduce the effects of spatial variations of "porosity" within each porous region.

The measurement system used for data acquisition is illustrated schematically in Figure 1. The transmitting and receiving transducers were oriented so that the insonifying beam was perpendicular to the surfaces of the sample and were aligned by viewing the received signal on a spectrum analyzer. A Metrotek MP215 wideband pulser was used to drive the transmitting transducer. The output of a MR106 wideband receiver was routed to a stepless gate and the 0.4 μsec gated signal was subsequently used as the input to the spectrum analyzer. A DEC PDP 11/73 computer was used to control the motor driven apparatus on a C-scan tank (in which the samples were placed for data acquisition) as well as to acquire the data from the spectrum analyzer for storage and subsequent analysis.

The signal loss through the composite laminate was obtained by normalizing the averaged acquired frequency spectrum with a calibration spectrum obtained from a water-only-path trace,

$$\text{Signal Loss} = \log[\text{calibration spectrum}] - \log[\text{sample spectrum}]. \qquad (1)$$

This method of log spectral subtraction removes systematic effects arising from the electromechanical response of the transducers and front-end electronics from the sample's spectrum. The normalized data were analyzed by performing a two-parameter polynomial fit about the center frequency $\bar{f}$ of the useful bandwidth,

$$\text{Signal loss} \simeq K_0 + K_1 \times (f - \bar{f}) \ , \qquad (2)$$

where K_0 is an estimate of the average signal loss over the useful bandwidth and K_1 is the rate of change of the signal loss with respect to frequency. This procedure is illustrated in Figure 2, where the signal loss of a typical spectrum is plotted as a function of frequency along with the appropriate two-parameter polynomial fit. The useable bandwidth of this system was 4 to 12 MHz.

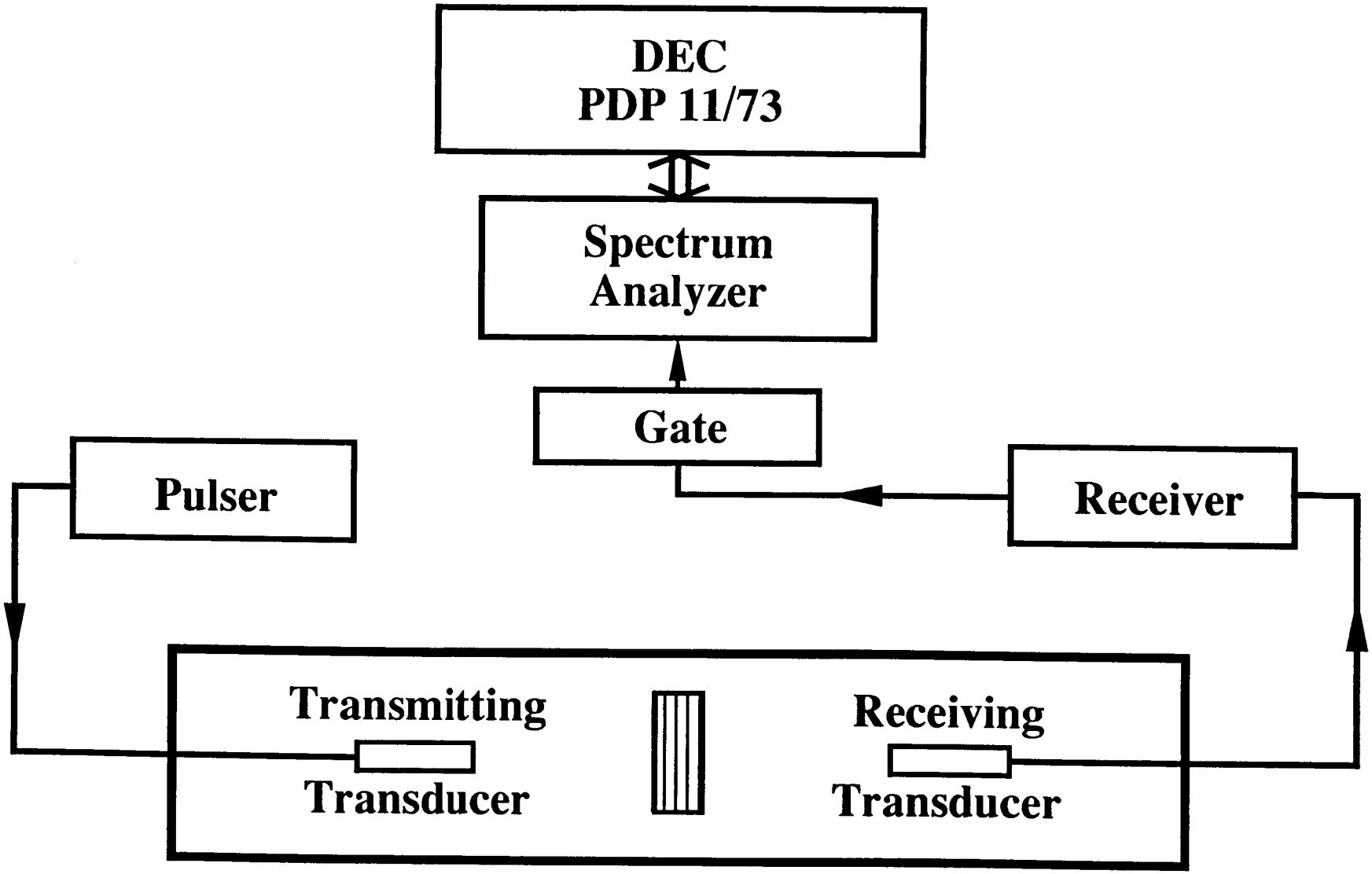

Figure 1: Block diagram of the transmission mode data acquisition system.

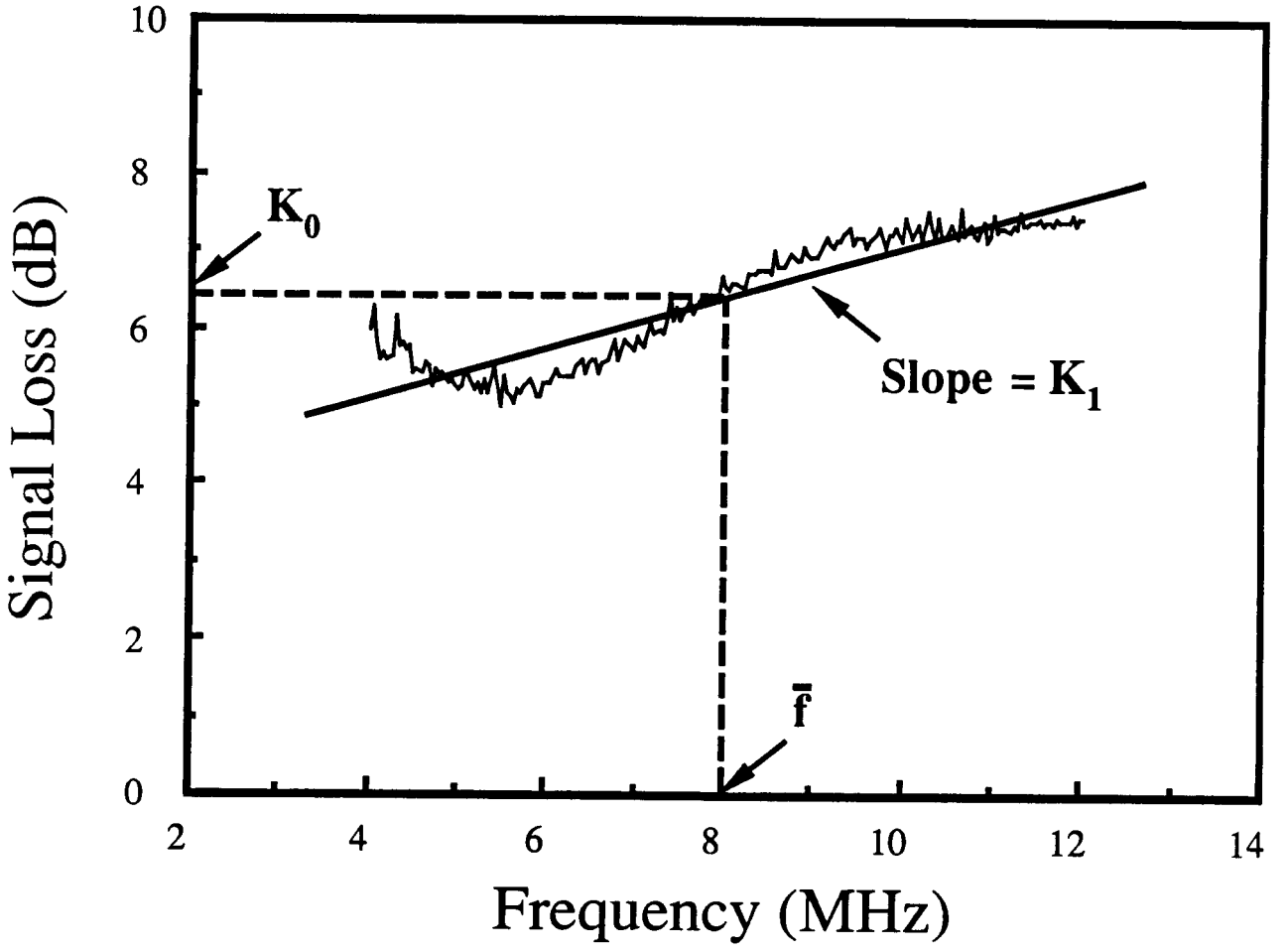

Figure 2: A typical signal loss spectrum and the corresponding two-parameter polynomial fit represented by Eq.(2).

2. Polar Backscatter Measurements

Backscatter measurements are performed with a single transducer that emits a short burst of ultrasonic energy and subsequently receives the ultrasonic signal backscattered from the specimen. In practice, the ultrasonic signal received at perpendicular incidence in the usual pulse-echo mode from a sample immersed in a coupling medium such as water is frequently dominated by the relatively uninteresting specular reflections from the front and back surfaces. In order to reveal more subtle variations in internal material properties it is useful to eliminate surface reflections. To achieve this goal the transducer was oriented at a polar angle different from zero degrees, i.e., at non-perpendicular incidence. This so-called polar backscatter approach, originally introduced by Bar-Cohen and Crane[2] and employed in several investigations reported from our laboratory in previous Progress Reports,[3,4,5] eliminates the strong surface reflections from the backscattered signal. Thus the specularly reflected signal is directed away from the transducer, which then receives only signals backscattered from inhomogeneities within the volume of the specimen.

Because the composites contain systematically-oriented fibers, the strength of the backscattered signal is dependent on the azimuthal orientation of the insonifying beam when a non-zero polar angle is used. This sensitivity to specific fiber orientations may be understood in a qualitative way on the basis of the following considerations (see Figure 3). Ultrasonic backscatter from cylindrical shaped fibers is largest for azimuthal angles ϕ for which the direction of insonification is perpendicular to the longitudinal axis of the fibers. Thus, for ultrasound insonifying a planar composite laminate at a non-zero polar angle θ, backscatter arising primarily from the individual fibers can be minimized by orienting the transducer such that the insonification is approximately parallel to the fiber axis. Polar backscatter was measured using a 10 MHz center frequency, 0.5 inch diameter, 4 inch focal length transducer. Each sample was scanned by translating the specimen over an 11 by 11 grid in 2 mm steps. Backscatter measurements were performed by insonifying the samples at a polar angle of 30° with respect to the normal of the sample surface, with the azimuthal angles centered at 0° with respect to the fiber orientation. At each site the azimuthal angle (ϕ) was varied in 5° steps from -10° to +10° and the resulting backscatter spectra averaged over site and azimuthal angle in order to minimize background variations not attributable to porosity.

Data were collected over the frequency range 4 to 12 MHz in 0.25 MHz steps using the system shown in Figure 3. Backscatter was measured quantitatively using a generalized substitution technique. The power spectrum of the backscattered signal was obtained using an analog spectrum analyzer. This power spectrum was then normalized

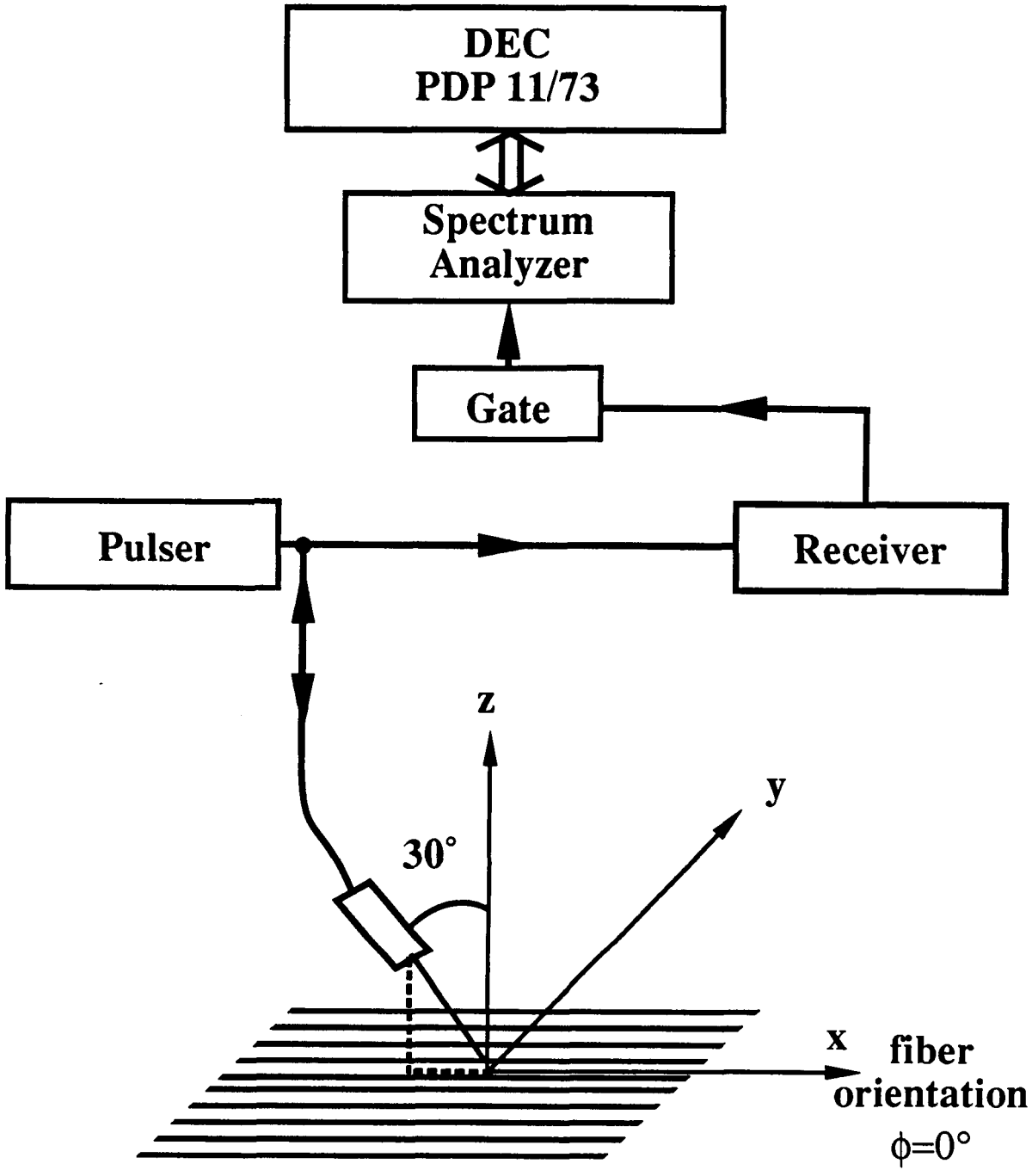

Figure 3: Block diagram of the polar backscatter mode data acquisition system.

to the power spectrum obtained in a second (calibration) measurement in which the specimen was replaced by a nearly perfect (flat stainless steel) ultrasonic reflector. The result of this normalization, the backscatter transfer function, is independent of the electromechanical efficiency of the transducer and the properties of the system electronics. The backscatter transfer function is a relative measure of the backscattering efficiency at a specified frequency.[6,7] The frequency average of the backscatter transfer function, termed the integrated backscatter, provides a useful index of backscatter efficiency over a finite bandwidth.[8] Frequency averaging over a broad bandwidth reduces the degrading influence of phase cancellation and other interference effects which can compromise the results of backscatter measurements. The integrated backscatter over the range 4 to 12 MHz is used as the basis for the quantitative backscatter correlation plots presented in the following Results Section of this Progress Report.

RESULTS

A. TRANSMISSION MODE MEASUREMENTS

Figure 4 displays the signal loss spectra and corresponding two-parameter polynomial fit for the samples with the minimum and maximum values of volume fraction of "porosity", 1% and 8%. The slope of the fit for the 8% sample is significantly larger than that for the 1% sample. It is this change in slope as a function of volume fraction that is used as the ultrasonic parameter to characterize the "porosity".

The results of the transmission mode measurements for each of the five samples are displayed on a scatter plot in Figure 5. The vertical axis represents K_1, the first order coefficient of the two-parameter polynomial fit (or the rate of increase of attenuation with respect to frequency), and the horizontal axis the volume fraction of "porosity". A clear trend exists between the slope of attenuation and the volume fraction of "porosity" as indicated in the figure. A linear least-squares fit performed on the data from this scatter plot yields a correlation coefficient of $R = 0.98$.

B. POLAR BACKSCATTER MODE MEASUREMENTS

The results of the reflection mode measurements for each of the five samples investigated in the present study are displayed on a scatter plot in Figure 6. The vertical axis represents the integrated polar backscatter and the horizontal axis represents the volume fraction of "porosity". A correlation coefficient of $R = 0.96$ was obtained by performing a linear least-squares fit to the data.

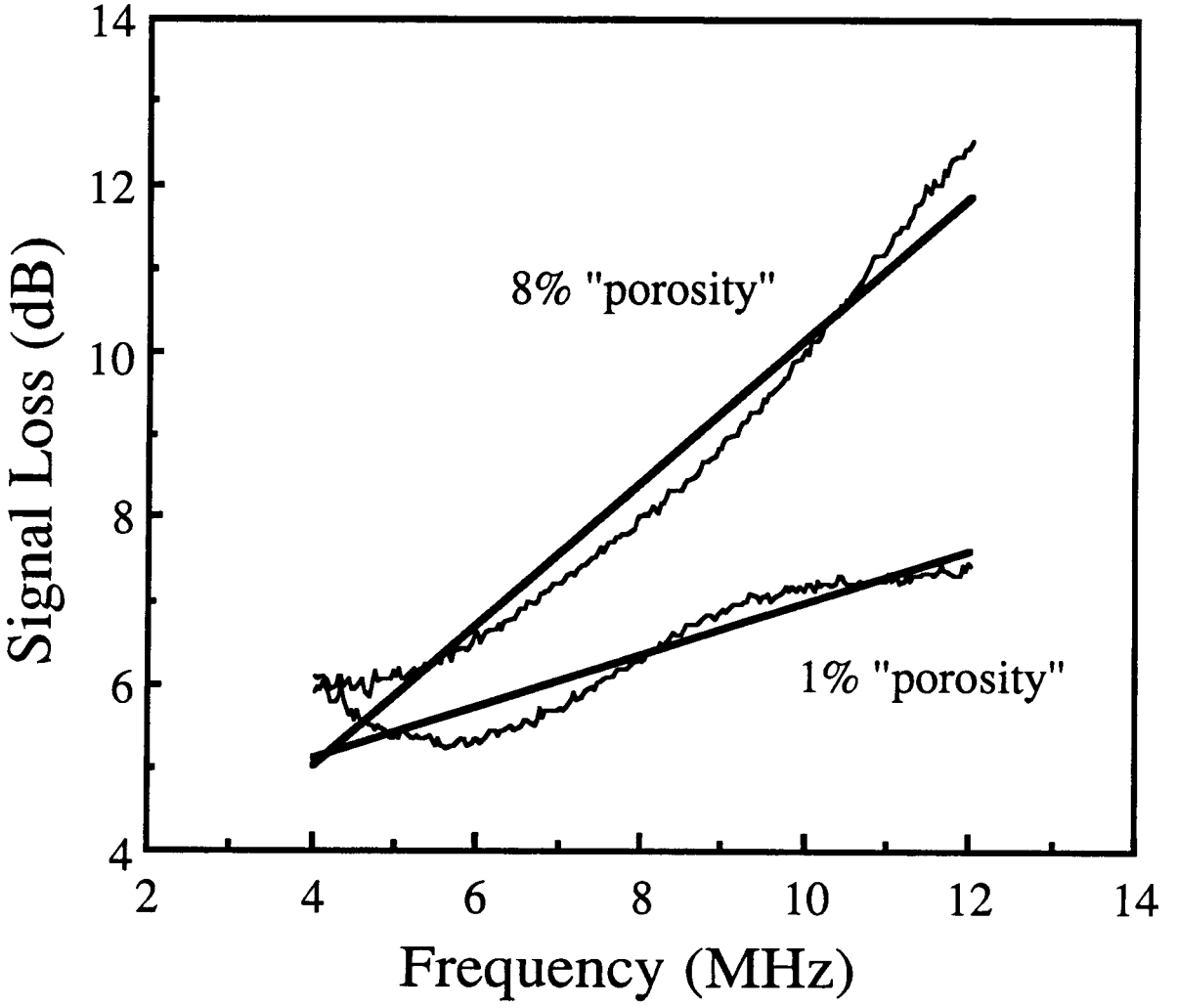

Figure 4: Spectra and corresponding two-parameter polynomial fits for 1% and 8% "porosity" samples plotted as functions of frequency.

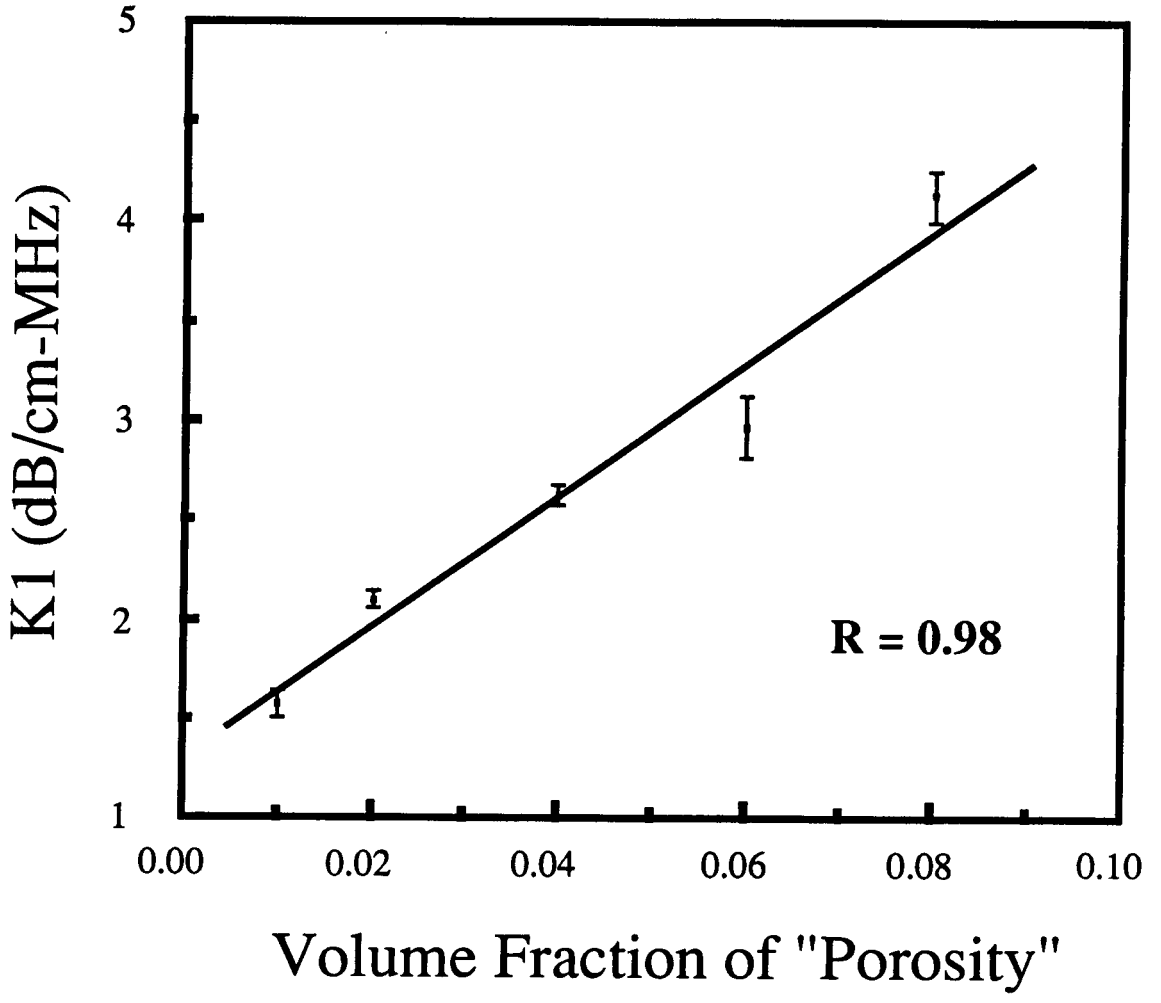

Figure 5: Correlation plot between the slope of attenuation and volume fraction of "porosity".

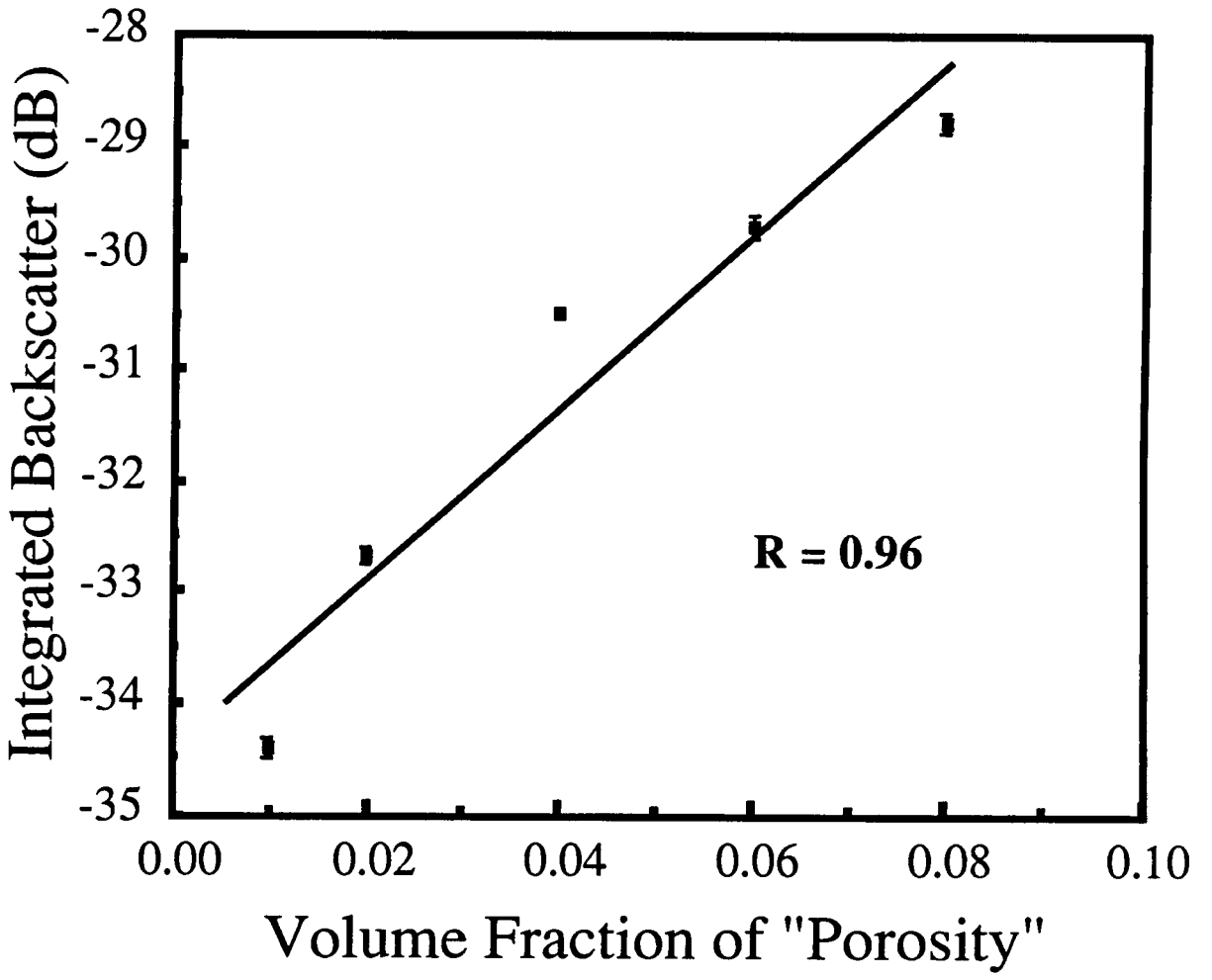

Figure 6: Correlation plot between the integrated polar backscatter and volume fraction of "porosity".

In summary, both the rate of increase with frequency of attenuation and integrated polar backscatter exhibited a good correlation ($R > 0.9$) with the volume fraction of "porosity". Attenuation based techniques are most readily applied under circumstances in which access to both sides of the specimen is feasible, whereas backscatter techniques lend themselves to measurements limited to single surface access. Results of these investigations suggest the potential value of these techniques for the nondestructive characterization of porosity in graphite/epoxy composites.

III. NEARLY LOCAL KRAMERS-KRONIG RELATIONS APPLIED TO POROUS EPOXY

The Kramers-Kronig relations are a pair of integral equations connecting the attenuation coefficient and the phase velocity.[9,10] Unfortunately, these exact relations require the evaluation of integrals over all frequencies in order to estimate the phase velocity from the attenuation coefficient and vice-versa. In 1978 O'Donnell, Jaynes, and Miller proposed a local approximation to the exact Kramers-Kronig relations which permits the dispersion, or change in phase velocity, to be estimated from the attenuation coefficient even when it is measured over a finite frequency range.[11,12] Rose and his collaborators have applied the exact Kramers-Kronig relations to the characterization of porosity in homogeneous and inhomogeneous media.[13,14,15] The additional attenuation due to pore scattering, i.e., the excess attenuation, was shown to contain information which permits the determination of pore radii and the volume fraction of porosity. We consider the application of the local approximation of O'Donnell, Jaynes, and Miller to the case of porous media. In particular, the dispersion due to pore scattering is predicted from the excess attenuation coefficient using a generalization of the local approximation.

RELATIONSHIP BETWEEN ATTENUATION AND PHASE VELOCITY

The Kramers-Kronig relations relate the real and imaginary parts of the frequency response function for any system satisfying these five assumptions: linearity, time-shift invariance, the energy in the system after any finite energy stimulus is finite, the time domain response to any real stimulus is itself real, and the system is causal. For acoustical systems these five assumptions appear to be satisfied at low amplitudes and lead to the following relations[11,12,16] between the attenuation coefficient, $\alpha(\omega)$, and the phase velocity, $C(\omega)$

$$\alpha(\omega) - \alpha(0) = -\frac{2\omega^2}{\pi}\int_0^\infty \frac{1/C(u) - 1/C(\omega)}{u^2 - \omega^2}du \ , \qquad (3)$$

and

$$1/C(\omega) = \frac{2}{\pi}\int_0^{\infty} \frac{\alpha/u^2 - \alpha/\omega^2}{u^2 - \omega^2} du \ . \tag{4}$$

In principle, these equations allow the attenuation coefficient to be calculated from the phase velocity and vice versa. However, the application of these equations requires that the attenuation coefficient (phase velocity) be known over all frequencies in order to calculate the phase velocity (attenuation coefficient). This requirement poses serious difficulties to the application of these relations to experimental data which can be known only over a finite bandwidth. One approach to this difficulty is to derive a local approximation to the exact relations. O'Donnell, Jaynes, and Miller[11, 12] proposed the following local approximation to the exact relations

$$\alpha(\omega) = \frac{\pi\omega^2}{2C(\omega)^2}\frac{dC(\omega)}{d\omega} \tag{5}$$

which may be integrated to obtain

$$1/C(\omega) - 1/C(\omega_0) = \frac{2}{\pi}\int_{\omega_0}^{\omega} \frac{\alpha(\omega')}{\omega'^2} d\omega' \ , \tag{6}$$

where ω_0 is a convenient reference frequency chosen to lie within the bandwidth of the experimental apparatus. This equation offers significant advantages over the exact Kramers-Kronig relations since it may be evaluated even when the attenuation data are known over only a finite frequency interval. For materials in which $C(\omega)$ is large compared to the change in velocity over the bandwidth of the apparatus ($C(\omega) - C(\omega_0)$) we may approximate Eq. (6) by

$$C(\omega) - C(\omega_0) = \frac{2C(\omega_0)^2}{\pi}\int_{\omega_0}^{\omega} \frac{\alpha(\omega')}{\omega'^2} d\omega' \ . \tag{7}$$

This approximation has been tested in homogeneous materials and found to agree well with experimental data.[11, 12]

MEASUREMENT OF ATTENUATION AND PHASE VELOCITY

Simultaneous measurements of the attenuation and dispersion in a 3.3 mm thick specimen of porous epoxy (6% volume fraction, 61 ± 18 microns pore radii) were made. A predication of the dispersion was obtained from the directly measured attenuation data and Eq. (7). The success of this approach may be judged by how well the direct and indirect predictions agreed. Figure (7) shows a block diagram of the experimental

apparatus which was used to measure the attenuation coefficient and dispersion. A sample of porous epoxy was immersed in a temperature controlled water bath so that it was in the far-field of the transducer. For our measurements a 25 MHz center frequency planar (0.25 inch aperture) transducer was used for both transmission and reception of broad-band ultrasonic pulses. The transducer was driven by a Metrotek MP215 pulser and the received pulses were amplified by a Metrotek MR106 receiver. The output of the receiver was fed into a sampling oscilloscope (Tektronix 2430) where it was digitized (at a 100 MHz sampling rate). The output of the oscilloscope was then transferred to a computer for storage and subsequent analysis.

The technique of the ultrasonic phase spectroscopy[17] is employed for the measurement of phase velocity and the technique of log spectral subtraction is used for the measurement of the attenuation coefficient. Two types of time domain traces are required for measurement of the attenuation coefficient and dispersion. The first is a reference trace acquired from a water-only-path. Subsequently, a sample trace is acquired from a specimen of either neat (i.e., pore-free) or porous epoxy. The analysis of these time domain traces is carried out as follows. First, the trace is windowed to remove uninteresting reverberations which may be present in the data. Several types of window functions have been investigated for this purpose. Although a Hanning window is suitable for applications in which only the attenuation is required, this type of window corrupts the phase data to such an extent that reliable estimates of phase velocity are not obtainable. For the data acquired in these studies, which typically contain well defined peaks separated by fairly wide baseline regions, a square wave window is sufficient. Next, an average baseline value is computed and subtracted from the entire data set. The time domain data is shifted so that its peak is centered at nearly zero time. This has the effect of removing a large linear ramp ($-\omega\Delta t$) from the resulting phase data, a direct consequence of the Fourier shift theorem.

The shifted data are Fourier transformed and the resulting complex frequency domain data are processed to obtain the attenuation coefficient and the dispersion. First, the phase of the complex frequency domain data is computed from the inverse tangent of the ratio of the real to the imaginary part of the complex frequency data. The data obtained in this fashion are next used as input to an algorithm which looks for 2π jumps in the data and removes them. Finally, the time ramp, which we removed implicitly by the time domain shift $-\omega\Delta t$, is added back to the unwrapped phase data to produce the true unwrapped phase. The phase is used in the calculation of the phase velocity according to the expression

$$v_s(\omega) = v_w \frac{2d\omega}{2d\omega + v_w\left[\phi_{ref}(\omega) - \phi_{sample}(\omega)\right]}, \qquad (8)$$

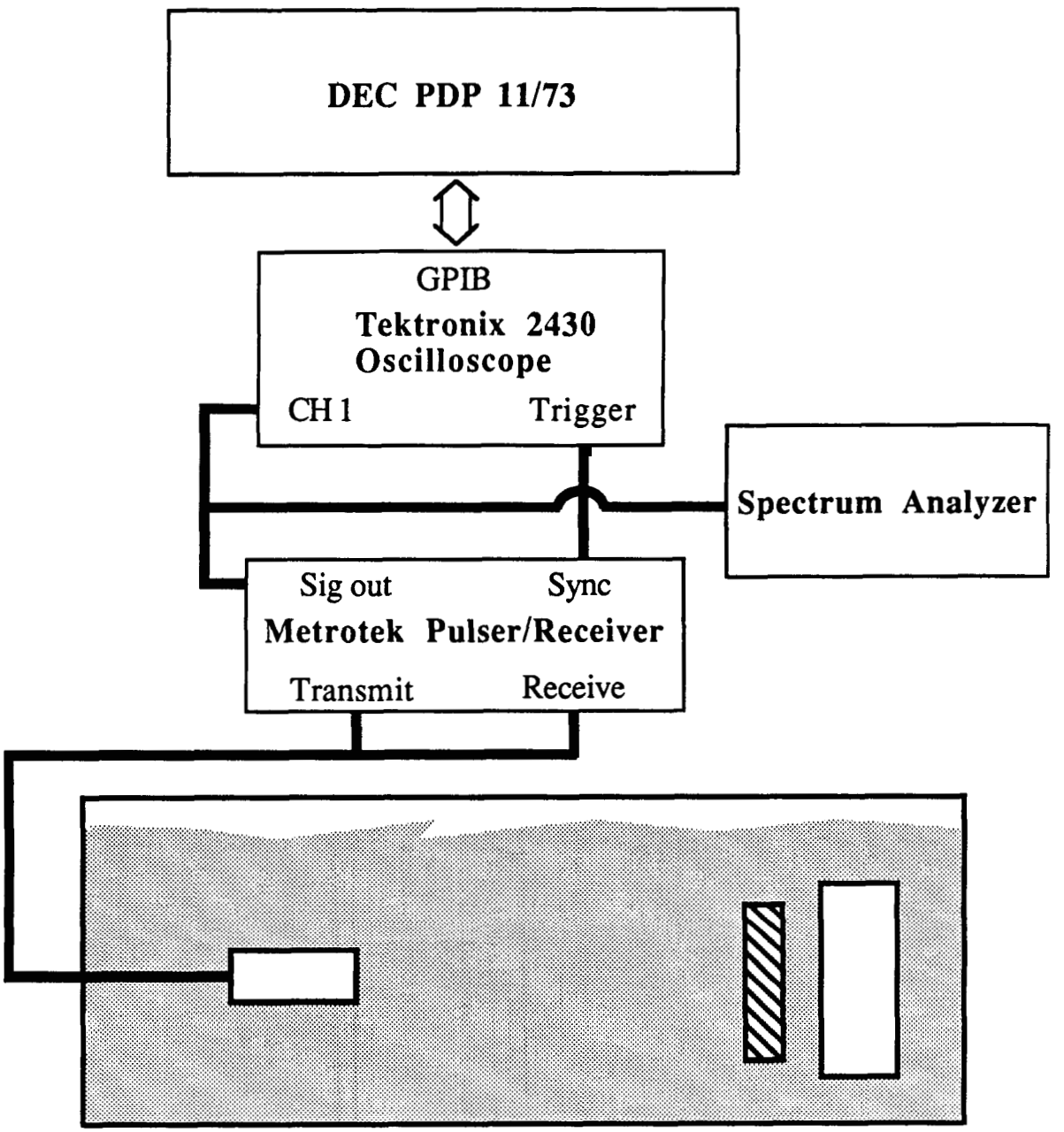

Figure 7: A diagram of the equipment used to measure attenuation and dispersion.

where the phases $\phi_{ref}(\omega)$ and $\phi_{sample}(\omega)$ are negative with the conventions we have chosen.

The magnitude data are obtained by computing the square root of the sum of the squares of the real and the imaginary parts of the complex frequency domain data. The magnitudes are then used to calculate the attenuation coefficient according to the formula

$$\alpha(\omega) = \left\{ \log_e\left[\begin{array}{c}\text{magnitude of trace of}\\ \text{the water–only path}\end{array}\right] - \log_e\left[\begin{array}{c}\text{magnitude of trace of}\\ \text{the epoxy specimen path}\end{array}\right] \right\} \Big/ 2d \ , \tag{9}$$

where d is the thickness of the sample. A typical attenuation coefficient plot, obtained from pore-free (neat) epoxy, is shown in Figure (8). Figure (9) shows a similar attenuation plot obtained from porous epoxy.

The experimental dispersion obtained from the neat specimen of epoxy using Eq. (7) is shown in Figure (10) by open boxes. Also shown in Figure (10), by solid black diamonds, is the prediction of phase velocity obtained from the measured attenuation coefficient (see Figure (8)) and Eq. (7). The two curves exhibit good agreement. A similar comparison for data obtained from the porous specimen of epoxy is shown in Figure (11). This figure also reveals good agreement between the direct measurements and the indirect estimates obtained from the local approximation.

RELATIONSHIP BETWEEN EXCESS ATTENUATION AND EXCESS DISPERSION

In order to perform a more sensitive test of the local approximation, measurements of the excess attenuation and excess dispersion due to pore scattering were conducted and an estimate of the excess dispersion was compared with the directly measured value. The excess attenuation may be obtained by subtracting the attenuation coefficient of the neat epoxy sample from the attenuation coefficient of the porous epoxy sample. A similar subtraction may be performed to obtain the excess dispersion. However, the excess dispersion and attenuation calculated in this straight-forward fashion were quite noisy, perhaps as a result of diffraction effects which differed in the water-only-path trace and the sample-trace.

The excess attenuation and excess dispersion can be obtained by a direct comparison between traces obtained through pore-free and porous samples. The resulting excess attenuation is presented in Figure (12). Inspection of the measured excess attenuation coefficient presented in Figure (12) shows that the following model may be

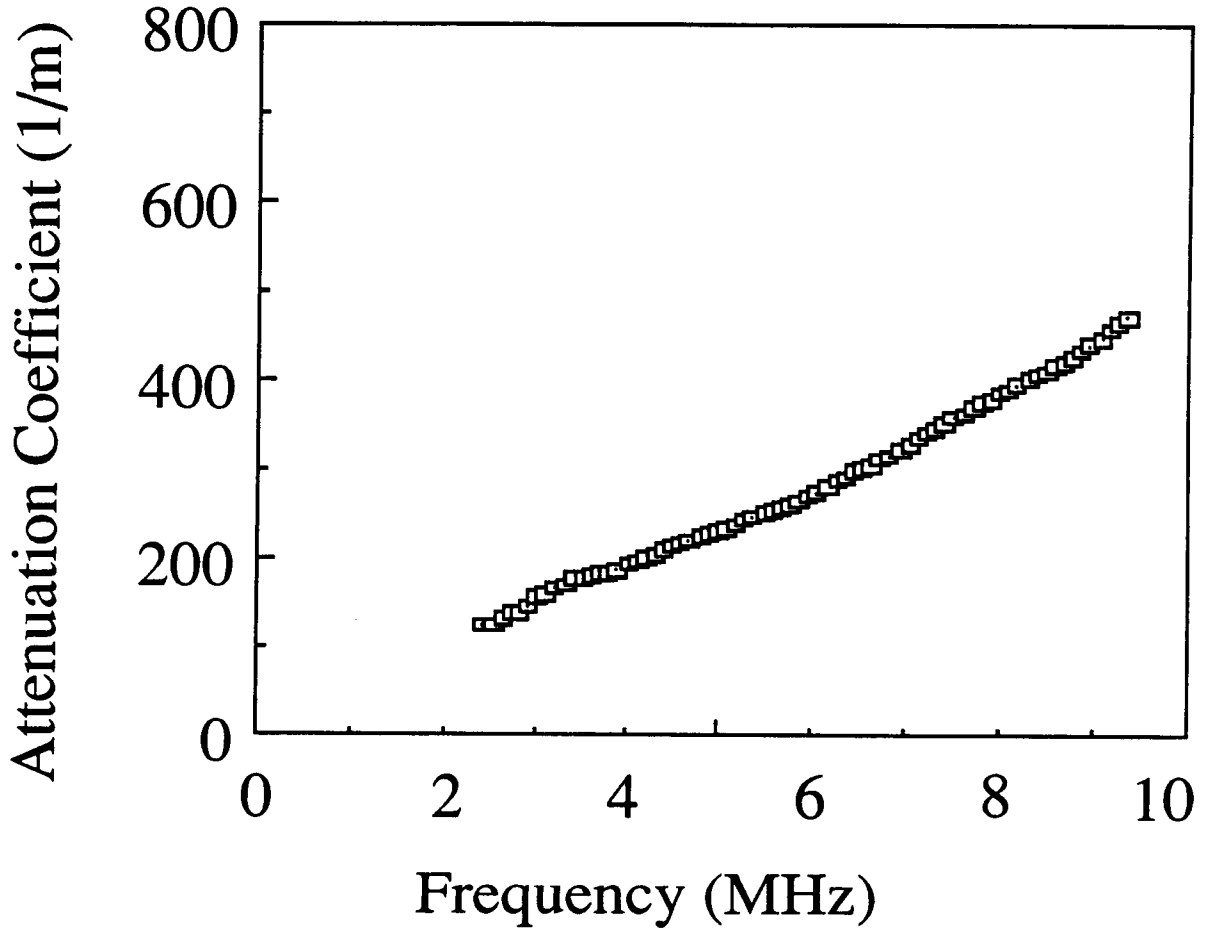

Figure 8: A plot of the attenuation coefficient obtained from pore-free (neat) epoxy.

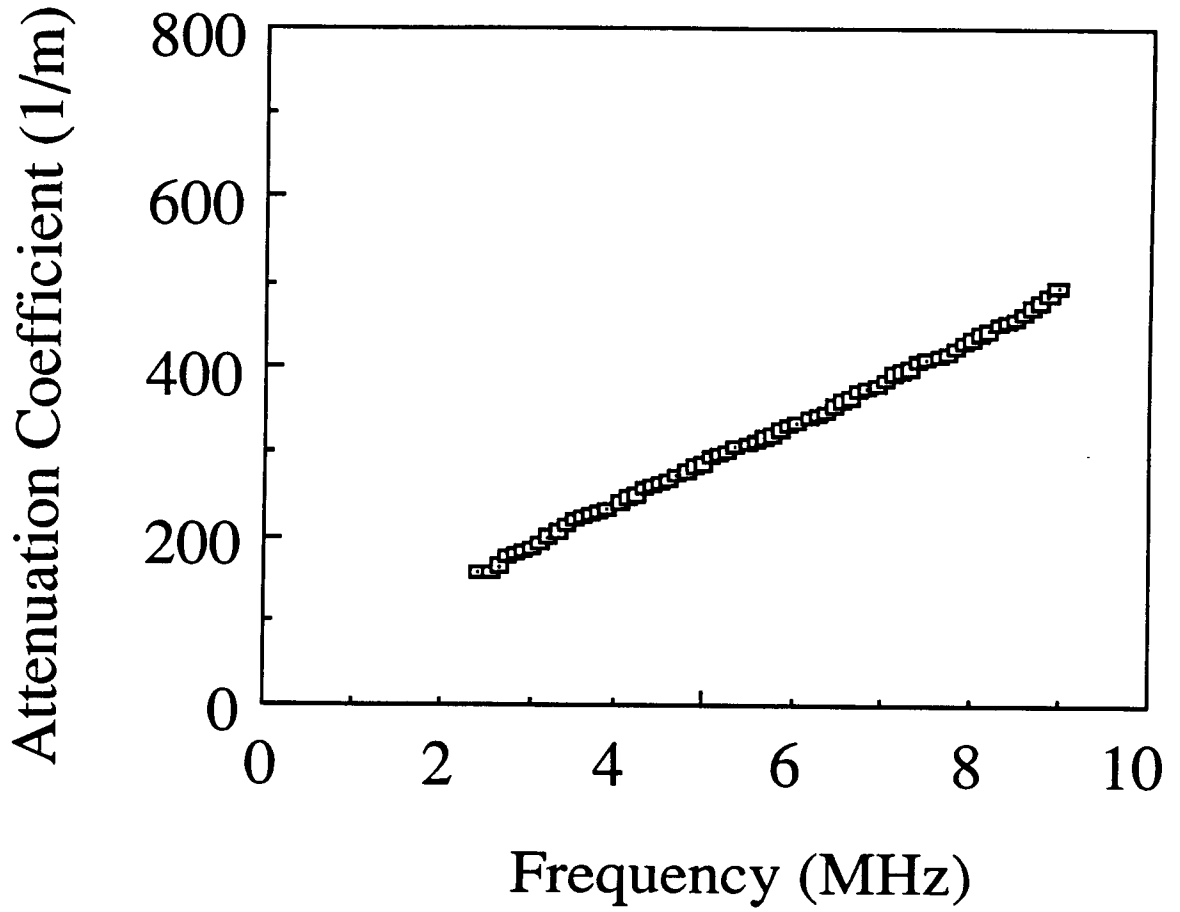

Figure 9: A plot of the attenuation coefficient for porous epoxy.

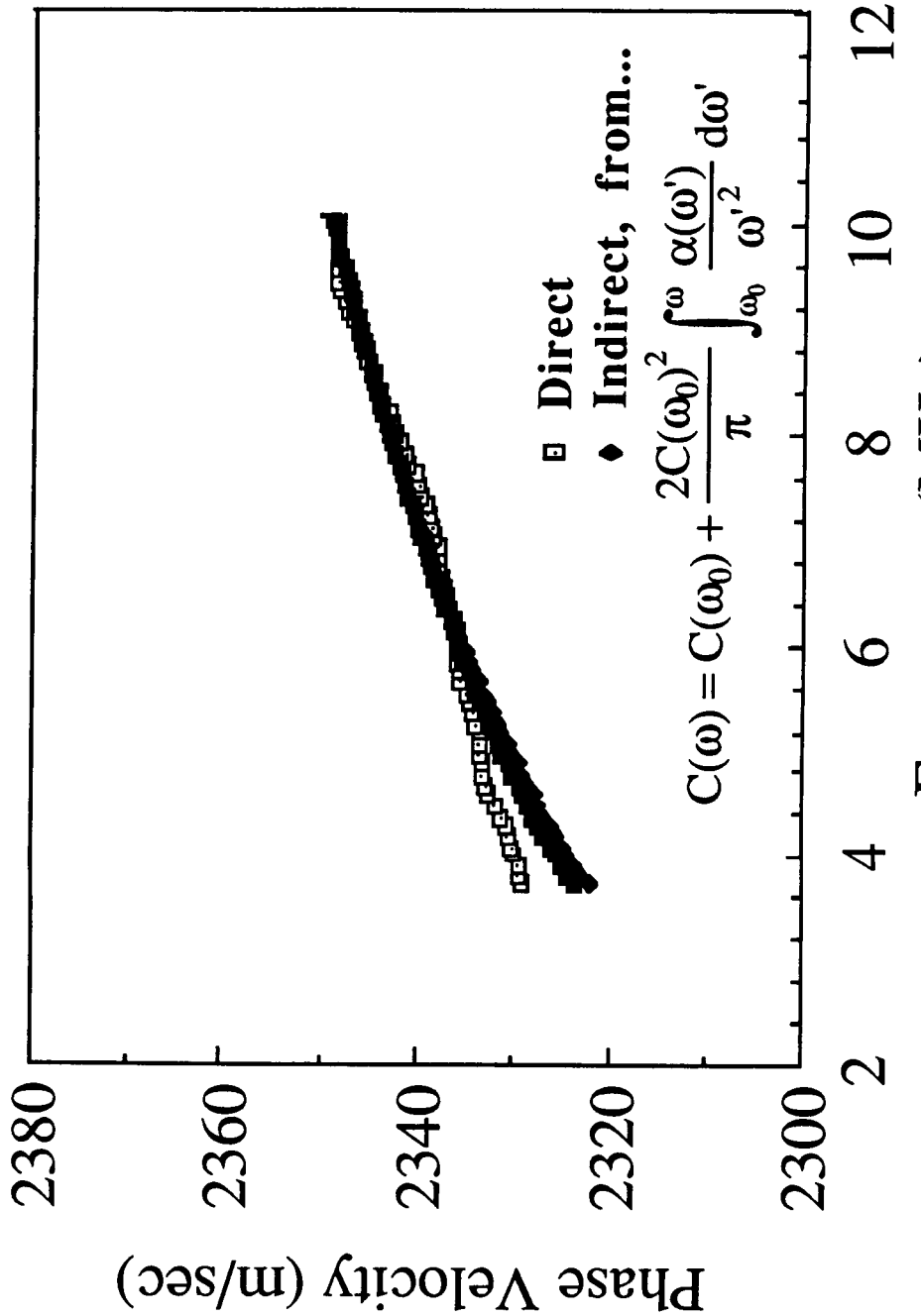

Figure 10: Two plots of phase velocity for neat epoxy. The open boxes are the measured data. The black curve is an estimate obtained from the measured attenuation data and the local approximation Eq. (7).

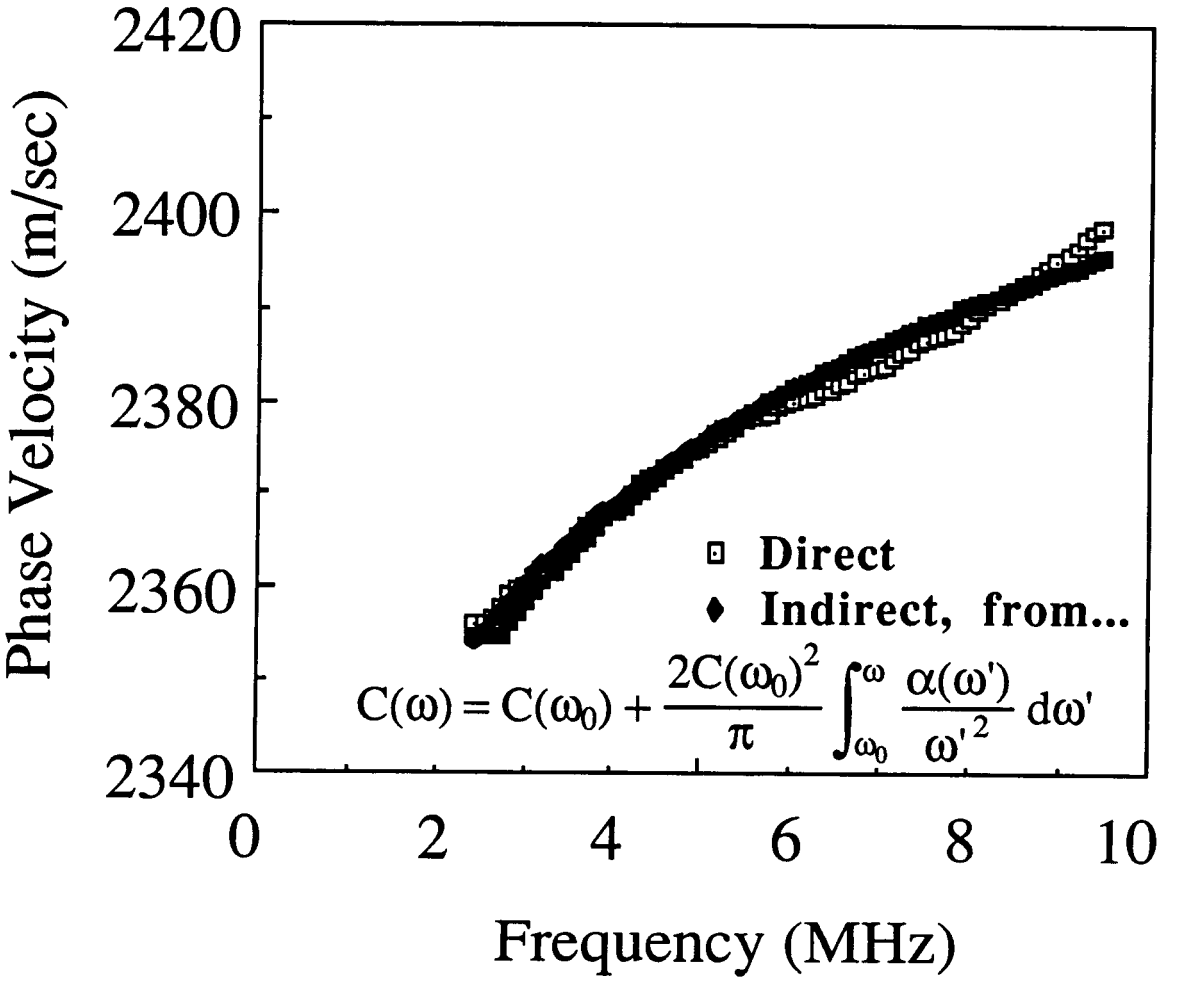

Figure 11: Two plots of phase velocity for porous epoxy. The open boxes are the measured data. The black curve is an estimate obtained from the measured attenuation data and the local approximation Eq. (7).

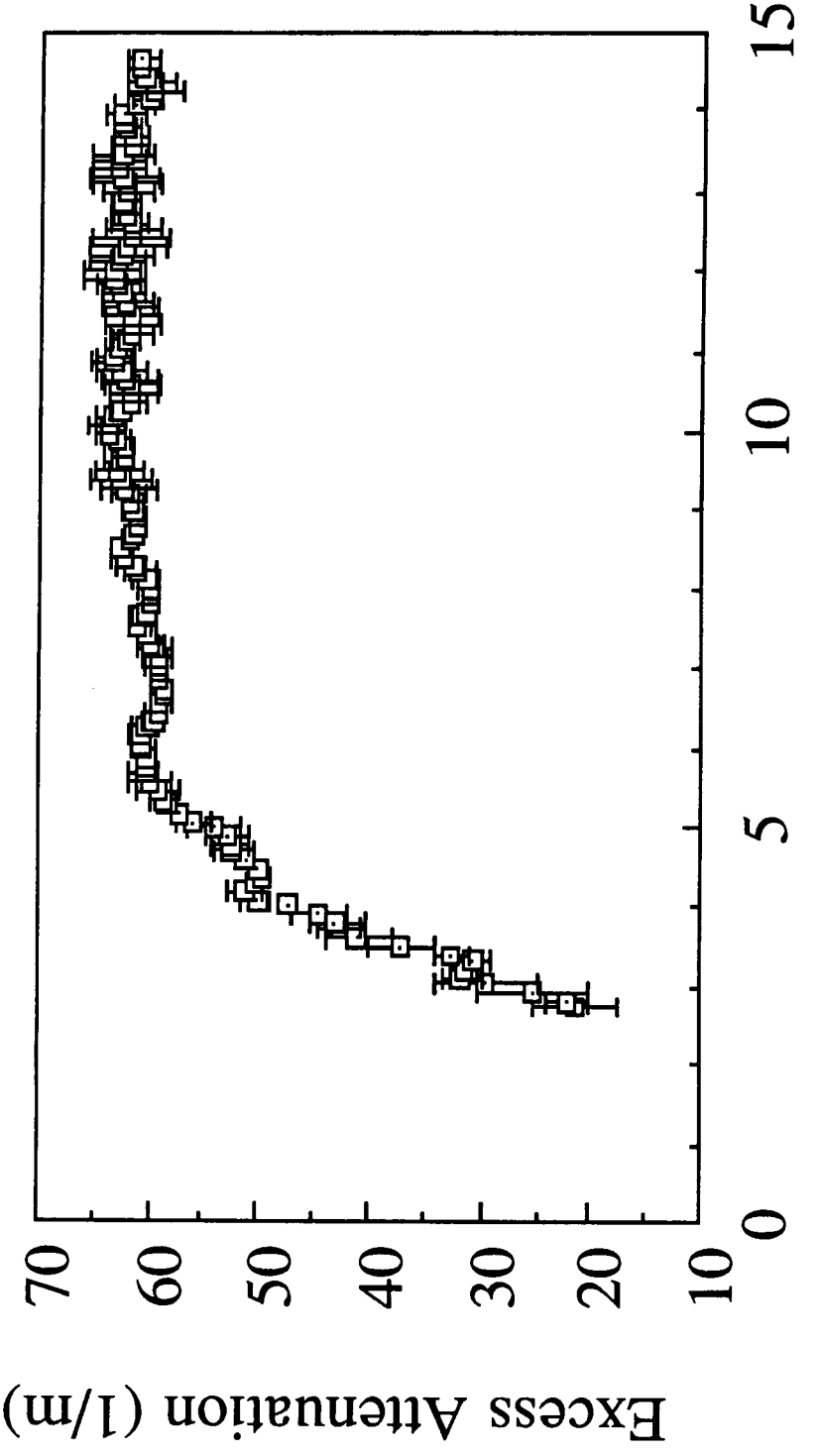

Figure12: A plot of the excess attenuation coefficient obtained for porous epoxy.

used to describe the excess attenuation coefficient

$$\alpha(\omega) = \begin{cases} \frac{\beta}{2\pi}\omega & \text{for } \omega < \omega_c \\ \frac{\beta}{2\pi}\omega_c & \text{for } \omega \geq \omega_c \end{cases} \tag{10}$$

where ω_c is the frequency at which the excess attenuation coefficient becomes frequency independent. Rose has predicted that this should occur at the frequency where ka≈1 and a is the pore radius.[18] Thus this break point provides an ultrasonic estimate of the pore radii in the specimen. The average pore radius for the sample used in this study was found (by optical measurements) to be 61±18 microns which agrees well with the value of ≈68 microns obtained using the measured excess attenuation data and Rose's criterion.

Before proceeding with the comparisons of direct and indirect estimates of excess dispersion it may be worthwhile to investigate the frequency dependence of the excess dispersion. Inserting the model equation, Eq. (10), for the excess attenuation coefficient into the local approximation Eq. (7) yields the following model frequency dependence for the excess dispersion.

$$\Delta C_{xs}(\omega) = \begin{cases} \frac{2C_0^2\beta}{\pi}\ln\left[\frac{\omega}{\omega_0}\right] & \text{for } \omega < \omega_c\,, \\ \frac{2C_0^2\beta}{\pi}\left\{\ln\left[\frac{\omega_c}{\omega_0}\right] + 1 - \frac{\omega_c}{\omega}\right\} & \text{for } \omega \geq \omega_c\,. \end{cases} \tag{11}$$

Thus one anticipates a logarithmic dependence for the excess dispersion in the low frequency, or ka < 1, region and a constant minus $1/\omega$ in the high frequency, or ka > 1 region. The predicted frequency dependence for Eq. (11) and for a continuation into the ka > 1 region of the low frequency logarithmic dependence are plotted in Figure (13) for $\beta = 5.0$ dB/MHz-cm, $\omega_c/2\pi = 5$ MHz, and $\omega_0/2\pi = 2$ MHz. Although both curves are concave downward, the divergence of Eq. (11) from the extrapolated low frequency behavior is apparent.

To obtain an expression for the excess dispersion without the use of a water-only-path, we subtract the equation (see Eq. (8)) for the phase velocity of sound in the neat sample from the equation for the phase velocity in the porous sample, which yields

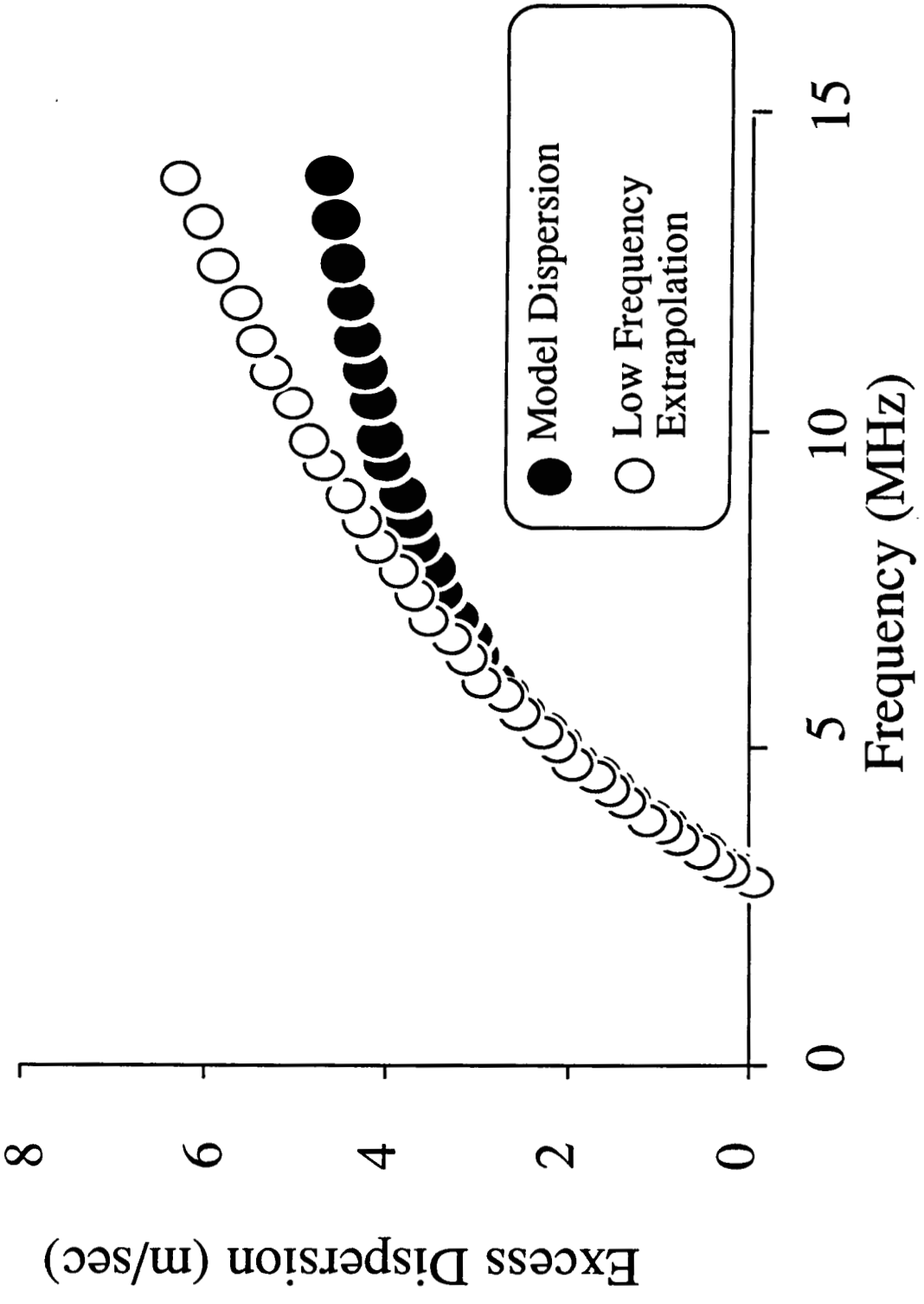

Figure 13: A plot of the model frequency dependence for the excess dispersion, given by Eq. (11), and an extrapolation of the low frequency behavior of Eq. (11) into the high frequency region.

$$\Delta C_{xs}(\omega) = \frac{v_n v_p}{2d\omega}\left[\phi_p(\omega) - \phi_n(\omega)\right] \quad . \tag{12}$$

The results of direct measurement of excess dispersion are presented in Figure (14). The excess dispersion is expressed relative to that at $\omega_0/2\pi = 4$ MHz. In addition to the open boxes which represent the directly measured excess dispersion, Figure (14) also includes a solid black line. This line was obtained by fitting the model for the excess attenuation coefficient, Eq. (10), to the experimentally measured excess attenuation and using the resulting parameter, β, to compute the low frequency behavior of the excess dispersion, see Eq. (11), which was then extrapolated into the $ka > 1$ region. An inspection of Figure (14) indicates that the extrapolation of the logarithmic behavior into the $ka > 1$ region diverges from the directly measured experimental values as expected.

In Figure (15) we show a comparison of the directly measured relative excess dispersion and an indirect estimate of the excess dispersion obtained from the directly measured excess dispersion data and the local approximation, Eq. (7). The satisfactory agreement illustrated in Figure (15) suggests that the local approximation remains useful even when the excess attenuation coefficient goes from a linear frequency dependence to a frequency independent behavior.

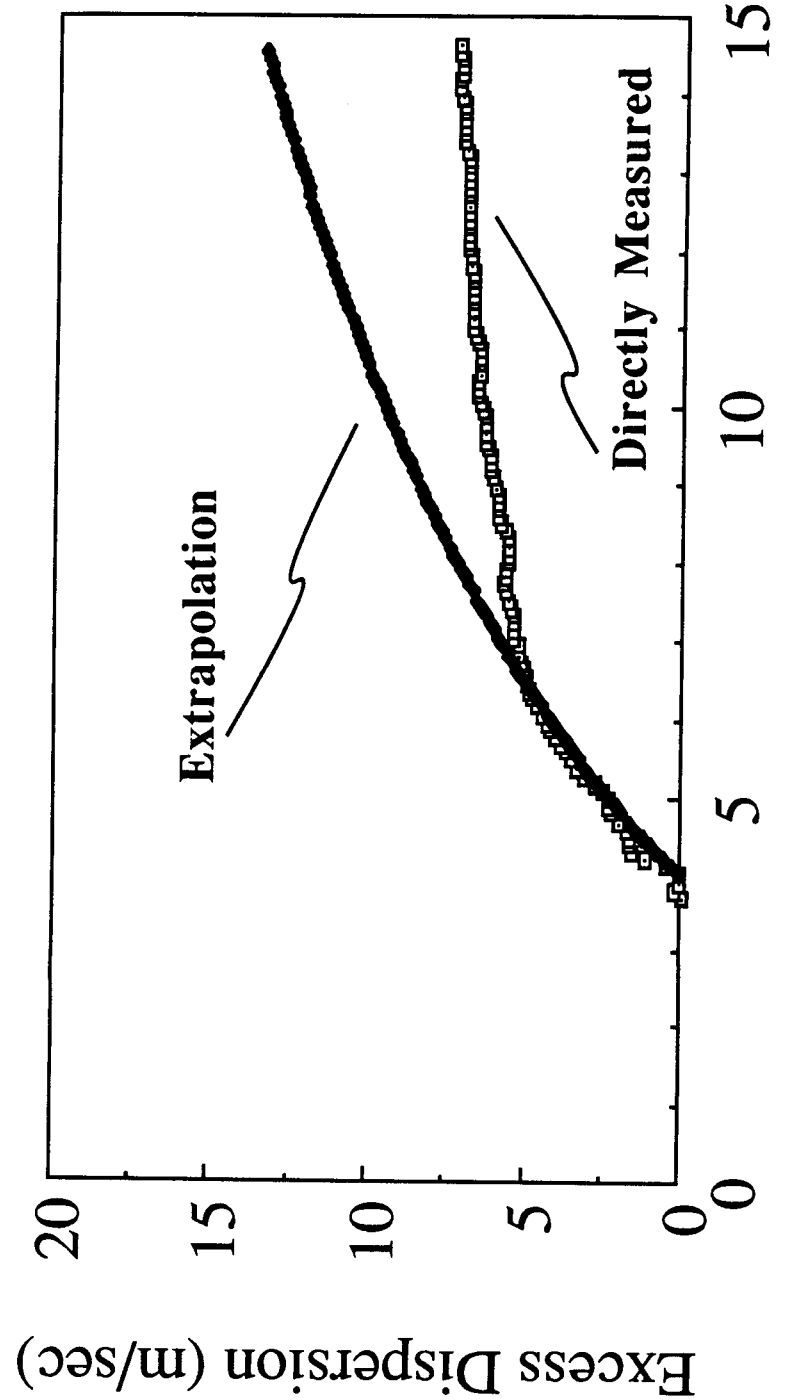

Figure 14: The open boxes represent the directly measured excess dispersion expression $\omega_0/2\pi = 4$ MHz. Also shown is an extrapolation of the low frequency behavior of the excess dispersion as predicted from the low frequency excess attenuation data and Eq. (10).

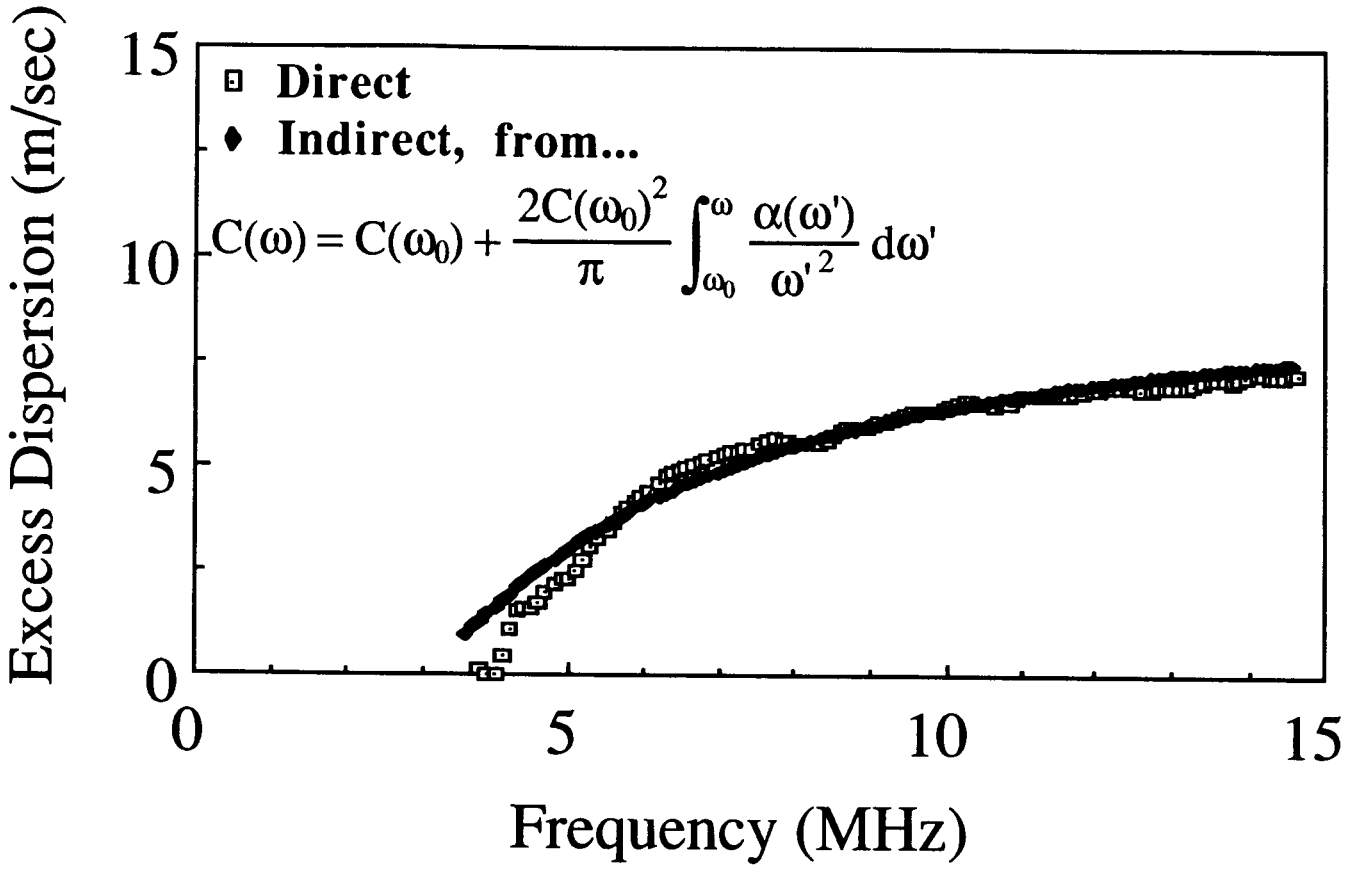

Figure15: Two plots of relative excess dispersion obtained from porous epoxy. The open boxes are the directly measured excess dispersion. The solid black line represents an estimate of the excess dispersion obtained from the directly measured excess attenuation data and Eq. (7).

References

1. Yoseph Bar-Cohen, *Nondestructive Characterization of Defects in Multilayered Media Using Ultrasonic Backscattering,* McDonnell-Douglas Corp., 1987. Douglas Paper 7781. Unpublished.
2. Y. Bar-Cohen and R.L. Crane, "Acoustic-Backscattering Imaging of Subcritical Flaws in Composites," *Materials Evaluation*, vol. 40, pp. 970-975, 1982.
3. Lewis J. Thomas III, Eric I. Madaras, and J.G. Miller, "Two-Dimensional Imaging of Selected Ply Orientations in Quasi-Isotropic Composite Laminates Using Polar Backscattering," *Proc. 1982 IEEE Ultrasonics Symposium*, pp. 965-970, 1982. (IEEE Cat. No. 82 CH 1823-4).
4. Earl D. Blodgett, Lewis J. Thomas III, and J.G. Miller, "Effects of Porosity on Polar Backscatter From Fiber Reinforced Composites," *Review of Progress in Quantitative Nondestructive Evaluation*, vol. 5B, pp. 1267-1274, 1986.
5. Earl D. Blodgett, S.M. Freeman, and J.G. Miller, "Correlation of Ultrasonic Polar Backscatter With the Deply Technique for Assessment of Impact Damage in Composite Laminates," *Review of Progress in Quantitative Nondestructive Evaluation*, vol. 5B, pp. 1227-1238, 1986.
6. M. O'Donnell and J.G. Miller, "Quantitative Broadband Ultrasonic Backscatter: An Approach to Non-Destructive Evaluation in Acoustically Inhomogeneous Materials," *J. Appl. Phys.*, vol. 52, pp. 1056-1065, 1981.
7. J.G. Miller, J.E. Perez, Jack G. Mottley, Eric I. Madaras, Patrick H. Johnston, Earl D. Blodgett, Lewis J. Thomas III, and B.E. Sobel, "Myocardial Tissue Characterization: An Approach Based on Quantitative Backscatter and Attenuation," *Proc. 1983 IEEE Ultrasonics Symposium*, pp. 782-793, 1983. (IEEE Cat. No. 83 CH 1947-1).
8. M. O'Donnell, D. Bauwens, J.W. Mimbs, and J.G. Miller, "Broadband Integrated Backscatter: An Approach to Spatially Localized Tissue Characterization In Vivo," *Proc. 1979 IEEE Ultrasonics Symposium*, pp. 175-178, 1979. (IEEE Cat. No. 79 CH 1482-9).
9. R. Kronig, "On The Theory Of Dispersion Of X-Rays," *J. Opt. Soc. Am.*, vol. 12, p. 547, 1926.
10. R. Kronig and H. A. Kramers, "Absorbtion And Dispersion In X-Ray Spectra," *Zeits f. Phys.*, vol. 48, p. 174, 1928.

11. M. O'Donnell, E.T. Jaynes, and J.G. Miller, "General Relationships Between Ultrasonic Attenuation and Dispersion," *J. Acoust. Soc. Am.*, vol. 63, pp. 1935-1937, 1978.

12. M. O'Donnell, E.T. Jaynes, and J.G. Miller, "Kramers-Kronig Relationship Between Ultrasonic Attenuation and Phase Velocity," *J. Acoust. Soc. Am.*, vol. 69, pp. 696-701, 1981.

13. James A. Rose, "Ultrasonic Characterization Of Porosity: Theory," in *Review of Progress in Quantitative Nondestructive Evaluation*, ed. D.E. Chimenti, vol. 4B, pp. 909-917, Plenum Press, 1985.

14. S. M. Nair, D.K.Hsu, and James A. Rose, "Ultrasonic Characterization Of Cylindrical Porosity: A Model Study," in *Review of Progress in Quantitative Nondestructive Evaluation*, ed. D.E. Chimenti, vol. 6B, pp. 1165-1184, Plenum Press, 1986.

15. L. Adler, J. H. Rose, and C. Mobley, "Ultrasonic Method To Determine Gas Porosity In Aluminum Alloy Casings: Theory And Experiment," *J. Appl. Phys.*, vol. 59, pp. 336-347, 1986.

16. A. I. Beltzer, "The High Frequency Response Of Random Elastic Composites," *Journal Of Applied Mathematics And Physics (ZAMP)*, vol. 36, pp. 336-347, Novbember 1978.

17. Wolfgang Sachse and Yih-Hsing Pao, "On the Determination of Phase and Group Velocities of Dispersive Waves in Solids," *J. Appl. Phys.*, vol. 49, pp. 4320-4327, 1978.

18. James A. Rose, "Ultrasonic Characterization Of Porosity: Theory," in *Review of Progress in Quantitative Nondestructive Evaluation*, ed. D.E. Chimenti, vol. 4B, pp. 909-917, Plenum Press, 1985.